RSC Advances

PAPER

View Article Online
View Journal | View Issue

Cite this: *RSC Adv.*, 2024, **14**, 19428

Synthesis of a resorcinol-based derivative as a corrosion inhibitor for low-carbon steel in 0.5 mol L^{-1} HCl medium: chemical, electrochemical, and theoretical aspects

Medhat M. Kamel, *[a] Mohamed A. Ghanem, *[b] Salah M. Rashwan,[a] Mostafa. A. Mahmoud,[a] Sameh A. El-Mekawy,[c] Khaled M. H. Mohammed[d] and Hoyida E. Ibrahim[a]

This work illustrated the synthesis of a new simple resorcinol derivative, 4,6-dimethoxyisophthalohydrazide (DMIH) and confirmed its structure using ^{1}H-NMR spectroscopy. The inhibiting performance of the DMIH compound in resisting the pitting action of a 0.5 mol L^{-1} HCl solution on low-carbon steel (LCS) was assessed. The newly synthesized compound had a simple structure and was dissolved in acidic media. The efficiency of the inhibitor was examined using chemical and electrochemical methods. The DMIH compound significantly decreased the rate of dissolution of LCS in HCl solution by adsorption. The adsorption was based on the Langmuir model. The DMIH compound is adsorbed on LCS *via* both chemisorption and physisorption. The DMIH compound is a mixed-type inhibitor. An inhibition efficiency (IE) of 83.8% was obtained using 300 ppm of the DMIH compound at 298 K. The IE decreased to 72% as the temperature increased to 328 K. When the concentration of DMIH increased from 50 to 300 ppm, the charge transfer resistance (R_{ct}) increased from 134.7 to 404.8 ohm cm^2, and the capacitance of the adsorbed layer decreased from 38 × 10^{-6} to 11 × 10^{-6} F cm^{-2}. The high IE of the synthesized inhibitor was validated by the quantum characteristics. Monte Carlo (MC) simulations revealed that the DMIH compound adsorbed to the LCS quite well. The presence of a protective film on the LCS specimen was verified by the scanning electron microscopy (SEM) and atomic force microscopy (AFM) results. DMIH has significant potential to function as a corrosion inhibitor, as indicated by the comparative study between its performance and that of previously reported compounds. Although the structure of the DMIH compound is simpler than that of other inhibitors, it has been proven to be more effective.

Received 9th May 2024
Accepted 11th June 2024

DOI: 10.1039/d4ra03404j

rsc.li/rsc-advances

1. Introduction

Corrosion is the reaction of a material with its environment that results in the deterioration of material properties. It is inevitable for most metals.[1] The process of corrosion affects every metallic object in our daily lives and all national infrastructure surfaces, including buildings, highways, chemical plants, wastewater treatment plants, bridges, and other surfaces. It has an adverse effect on the environment.[2,3] It is possible to prevent, or at least minimize, corrosion by using appropriate materials, changing the corrosive environment, using inhibitors, using superior designs, applying coatings, and using cathodic and anodic protection techniques.[4]

Low-carbon steel (LCS) is the principal engineering material used to build oil and gas production systems, vessels, and pipelines for transporting water, chemicals, and petroleum products. It is frequently used because of its excellent mechanical characteristics and reasonable price.[5] HCl acid is used in a variety of industrial operations, particularly in the petroleum industry, acid cleaning, and acidizing. It acts aggressively against metallic structures, which results in financial losses.[6]

It has been shown that one of the most efficient ways to control the corrosion process is to utilize an inhibitor because it is a realistic, economical, and effective strategy.[7] Various organic and inorganic substances have been successfully employed as carbon steel corrosion inhibitors in acidic corrosive media.[8] The molecular structure of the corrosion inhibitor, which is crucial for its ability to adsorb to the surface of the alloy or metal and form a protective coating, determines how well the

[a]*Department of Chemistry, Faculty of Science, Suez Canal University, Ismailia 41522, Egypt. E-mail: medhat_darwish@science.suez.edu.eg; Fax: +20 643230416; Tel: +20 1004482037*

[b]*Department of Chemistry, College of Science, King Saud University, Riyadh 11451, Saudi Arabia*

[c]*Department of Physics and Mathematics, Faculty of Engineering, Port Said University, Port Said, Egypt*

[d]*School of Chemistry, University of Southampton, Southampton SO17 1BJ, UK*

inhibitor controls corrosion damage. The organic inhibitors usually contain oxygen, sulfur, and nitrogen heteroatoms, as well as π-electrons and specific functional groups like $-NH_2$, –COOH, or –OH.[7,8] These enable the inhibitors to strongly interact with the metal and form a potent protective film at its surface, preventing direct contact with the aggressive medium. Adenine, triazoles, thiazoles, imidazole, benzimidazoles, benzotriazoles, purines, and ionic liquids are examples of heterocyclic organic molecules that can also be considered favorable organic inhibitors.[9] The most frequently used inhibitors for protecting carbon steel, especially when hydrochloric acid is present, are organic inhibitors.[10]

Many authors have investigated the corrosion of steel in different corrosion media.[5,10–28] A combination of sodium dodecyl sulfate bromide (SDS) and cetyltrimethylammonium bromide (CTAB) was used as a corrosion inhibitor in a 3.5% NaCl solution.[11] Both cathodic and anodic reaction rates were decreased by the inhibitor. Another study employed sodium gluconate and CTAB for galvanized steel in a 3.0% NaCl solution.[12] The effect of coated-mild steel with SDS inhibitor and Mo in a 3.5% NaCl solution was studied by Farahmand *et al.*[13] At 0.8 mM SDS and 75 mm thickness of Mo, excellent effectiveness was reported. Nam *et al.*'s investigation[14] focused on the corrosion inhibition caused by cerium hydroxycinnamate derivatives on mild steel in 0.6 M NaCl. The investigated compounds decreased the corrosion rate of mild steel. A novel imidazole derivative, (*N*,*N*′*E*,*N*,*N*′*E*)-*N*,*N*′-(thiophene-2,5-diylbis(methanylylidene))bis(1*H*-benzo[*d*]imidazole-2-amine), was synthesized and characterized by Al-Najjar and Al-Baitai.[10] They evaluated the new compound as an inhibitor for the pitting of LCS in a 0.1 M HCl solution, employing different techniques. The optimum inhibition efficiency of the compound at 0.5 mM was 96%.

α-Aminophosphonate was utilized as an innovative corrosion inhibitor for LCS in corrosive media containing HCl and H_2SO_4 acid solutions.[5] The investigated compound suppressed the dissolution of LCS in the studied acid solution. At 180 ppm, the maximum inhibitory efficiency was attained. Ahmed *et al.*[15] investigated the effects of six synthetic heterocyclic compounds on the corrosion inhibition of mild steel in 0.5 M hydrochloric acid by the weight loss method. They reported that the inhibition efficacy exceeded 95%. Khadom *et al.*[16] conducted a study on the corrosion inhibition of N80 steel in 0.5 M HCl acid using (*S*)-6-phenyl 2,3,5,6 tetrahydroimidazo[2,1-b] thiazole. The inhibition efficacy was more than 95%. The inhibitor was adsorbed according to the Langmuir adsorption isotherm model. 1-[(5-Phenyl-1,3,4-oxadiazol-2-yl)thio] acetone (POTA) compound was synthesized and examined in 1 M hydrochloric acid as a potential novel corrosion inhibitor for LCS.[17] FTIR and NMR measurements were used to diagnose the POTA compound. The adsorption layer that formed on the LCS surface was responsible for the inhibitor's performance. Using a grinding process, six new triazole compounds were created from substituted benzoic acid and thiocarbohydrazide.[18] Triazole compounds were examined in 0.5 M HCl as a corrosion inhibitor for LCS. The compounds exhibited encouraging corrosion-inhibiting properties when applied to LCS in acidic solutions.

In our laboratory, we have conducted various scientific papers to combat the corrosion of LCS in acidic environments, employing ionic liquids,[19] organic inhibitors,[20–22] inorganic inhibitors,[23] polymers,[24] Gemini-type surfactants,[25] Schiff bases,[26] and plant extracts.[27,28]

The aim of the present work is to synthesize, characterize, and assess the inhibiting behavior of a novel compound (DMIH) for LCS in a 0.5 mol L^{-1} HCl solution. The main objective of this study is to investigate the performance of the DMIH compound in a 0.5 mol L^{-1} HCl solution to reduce the corrosion rate of LCS. Potentiodynamic polarization (PDP), weight loss (WL), and electrochemical impedance spectroscopy (EIS) techniques were employed. The relationship between temperature, thermodynamic variables, corrosion rate, and IE was estimated and studied. SEM and AFM were used to investigate the surface of LCS. Furthermore, the interaction between DMIH molecules and the LCS surface was investigated using Monte Carlo simulations and density functional theory (DFT).

2. Experimental details

2.1 Materials and solutions

Low-carbon steel sheets with the composition (wt%) of 0.20 C, 0.60 Mn, 0.04 P, 0.003 Si, and the remainder of Fe were used in the present study. The steel sheets were used without annealing processes. At 50, 100, 150, 200, 250, and 300 parts per million (ppm), the synthesized inhibitor was used. To prepare the corrosive medium, a fine-grade 37% HCl acid was diluted to 0.5 mol L^{-1} HCl solution by distilled water. All chemicals used in this study were of high purity (99.5%) and purchased from Sigma-Aldrich. Saturated calomel (SCE) and Pt gauze were used as the reference and counter electrodes, respectively.

2.2 The DMIH compound: synthesis and characterization

The DMIH was synthesized by the reaction of 11.3 g of 4,6-dihydroxy-isophthalo hydrazide with 50 mL of Me_2SO_4. The mixture was dissolved in 300 mL of acetone, and 82.8 g of K_2CO_3 was added. Subsequently, the mixture was refluxed for 96 hours. Once the mixture cooled to room temperature, 100 mL of CH_2Cl_2 was added, and the solution was agitated for 30 minutes. The insoluble residue was filtered, and the organic layer was thoroughly washed with water. After evaporation of the solvent, the residue was washed with water and dried under vacuum. The yield was 92%. Table 1 shows the chemical structure, IUPAC name, molecular formula, and molecular mass of the synthesized DMIH compound. Scheme 1 demonstrates the schematic preparation of the DMIH compound. ^{1}H-NMR (DMSO-d_6) was performed using a Bruker Advance III-400 MHz NMR spectrometer.

2.3 Weight loss (WL) methods

WL experiments were performed in accordance with ASTM-G1.[29] Polished carbon steel sheets (2 × 2 × 0.1 cm^3) were completely submerged in 100 mL of 0.5 mol L^{-1} HCl solution

Table 1 Chemical structure, IUPAC name, molecular formula, and molecular mass of the synthesized organic compound DMIH

Compd.	IUPAC name	Chemical structure	Molecular formula	Molecular mass (g mole^{-1})
DMIH	4,6-Dimethoxyisophthalohydrazide	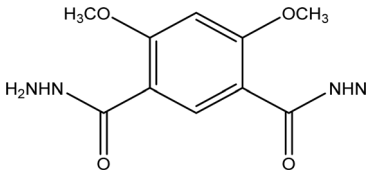	$C_{10}H_{14}N_4O_4$	254.24

Scheme 1 Synthesis of DMIH based on 4,6-dihydroxyisophthalohydrazide (DIH).

for 24 hours at 298–328 K in the absence and presence of different concentrations (50–300 ppm) of the synthesized compound. After that, the samples were dried, cleaned, and weighed. To obtain reliable results, the experiment was conducted three times. The results are presented as the mean weight loss (mg) ± standard deviation (SD).

2.4 Electrochemical studies

The EC-LAB software and a Biologic SP-150 potentiostat/galvanostat were used to conduct the electrochemical procedures. A typical electrolytic-jacketed glass cell (250 mL) employed a three-electrode setup: platinum gauze served as the counter electrode, LCS as the working electrode, and SCE as the reference electrode. All the measurements were performed at 298 ± 1 K. With a 1 cm^2 surface area available for solution contact, the LCS electrode was sliced into a cylindrical shape and coated with epoxy resin. Before any experiments were conducted, the LCS electrode was abraded with emery paper ranging in grade from 200 to 1500 and then washed with distilled water and acetone. The LCS electrode was immersed in the test solution for 40 minutes to reach the steady state (E_{ocp}). The PDP curves were scanned from −500 to −250 mV (SCE) regarding E_{ocp}, using a scan rate of 0.2 mV s^{-1}.

Tests using electrochemical impedance spectroscopy (EIS) were conducted using a sinusoidal wave with an amplitude of 5 mV at frequencies ranging from 100 kHz to 0.05 Hz. Each experiment was conducted in triplicate to ensure the reliability of the electrochemical tests.[30–32] The results were collected using a personal computer. Origin 2018 was used to display, graph, and fit the data.

2.5 Surface morphology study

In the absence and presence of 300 ppm of a synthetic inhibitor, the surface morphology of LCS was examined. The LCS surface was investigated using atomic force microscopy (AFM) (Keysight 5600LS big stage, USA) and a JOEL JSM-6510 LV scanning electron microscopy (SEM).

2.6 Computational study

DFT and MC simulations were theoretically used to reveal the optimum molecular structure of the synthetic inhibitor, besides the mechanism of inhibition. The DFT/6-31+G(d, p) basis set and the 3-21G(d) basis set of the Monte Carlo MP2 functional were used to calculate the quantum chemical parameters for all atom simulations.

3. Results and discussion

3.1 ^{1}H-NMR spectroscopy

Fig. 1 shows the ^{1}H-NMR spectra (DMSO-d$_6$, 400 MHz) of the DMIH compound. A singlet peak appeared at 2.519, assigned to 4H in the 2 (NH_2) group. However, that appeared at 3.943 owing to six hydrogens in the 2 (OCH_3) group. A singlet peak appears at 6.756, ascribed to the 1H proton in the benzene ring, and a singlet peak at 8.281 because of the 1H proton in the benzene ring. A sharp peak at 9.089 was assigned to a 2H proton in the 2(NH) group.

3.2 WL study

3.2.1 Effect of DMIH concentration. WL measurements provide remarkably precise data regarding an inhibitor compound's efficacy when compared to other tests. Therefore, it enables the accompanying corrosion statistics to accurately reflect service conditions.[33] In 0.5 mol L^{-1} HCl solutions, the WL of LCS was examined in relation to immersion time without and with different concentrations (50–300 ppm) of the DMIH compound at 298–328 K. Fig. 2 shows the effect of increasing the concentration of the DMIH compound on the WL of LCS at 298 K. The weight loss per unit time for each line in the figure reflects the rate of corrosion of LCS at a certain concentration. The corrosion rate (k), inhibition efficiency (IE_w), and surface coverage (θ) by the DMIH compound are calculated by eqn (1)–(3), respectively, for LCS in the blank solution and in the presence of different concentrations of the DMIH compound.[34]

$$k = \frac{\Delta W}{At} \quad (1)$$

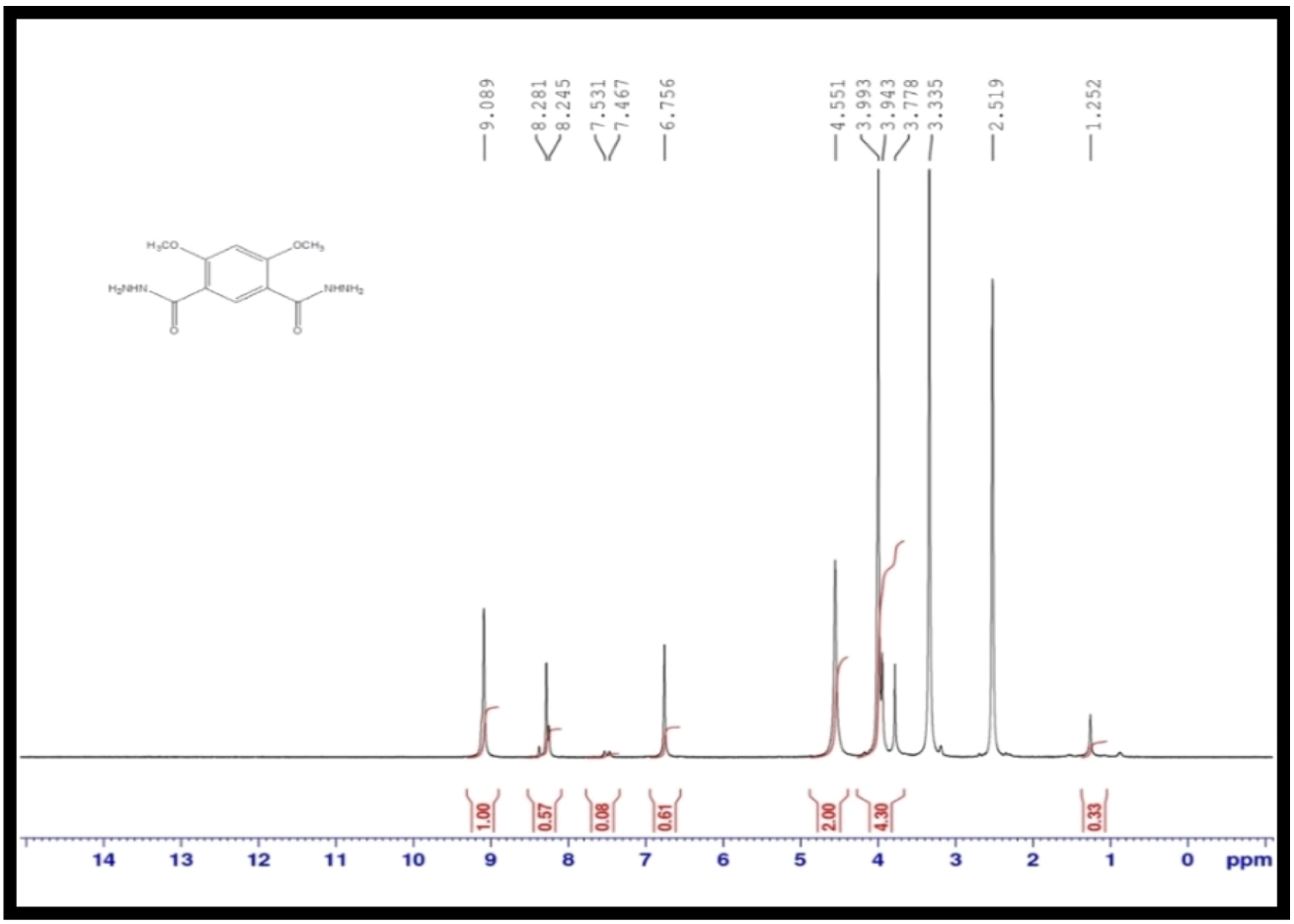

Fig. 1 ^{1}H-NMR of the DMIH compound.

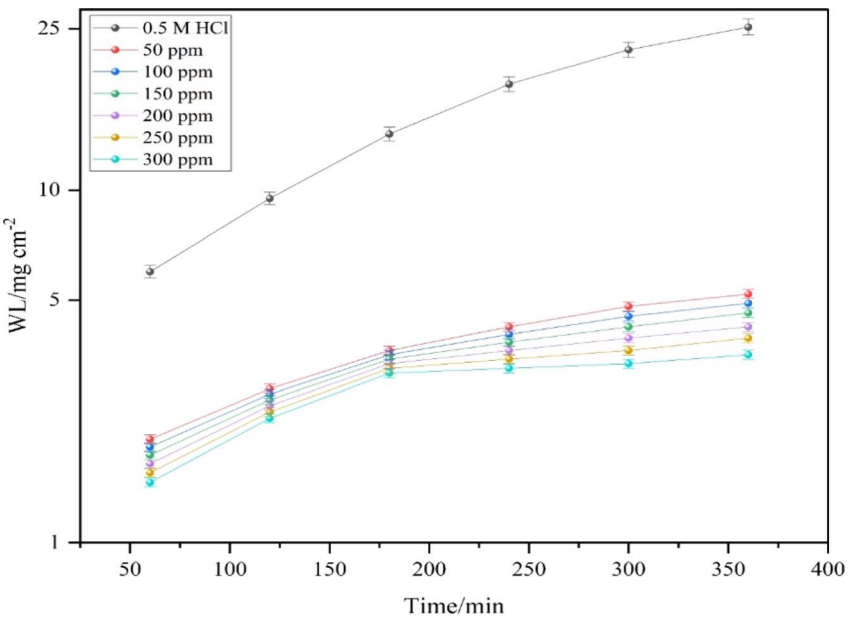

Fig. 2 WL curves for the corrosion of LCS in 0.5 mole L^{-1} HCl in the absence and presence of different concentrations of the DMIH compound at 298 K.

where ΔW is the weight loss of the LCS coupon in kg, A is the surface area of the LCS coupon in m^2, and t is the submersion time in seconds.

$$IE_w = \left(1 - \frac{W_{inh}}{W_{corr}}\right) \times 100 \quad (2)$$

where W_{corr} and W_{inh} are the WL of the LCS coupons without and with the inhibitor, respectively.

$$\theta = \left(1 - \frac{W_{inh}}{W_{corr}}\right) \quad (3)$$

Table 2 shows the obtained WL data for LCS after immersion for 240 minutes in 0.5 mol L^{-1} HCl without and with different concentrations of the synthesized inhibitor at varying temperatures. At 298 K and in the presence of 50 ppm of the DMIH compound, the inhibition efficiency is 63.9%. As the concentration of the inhibitor increases to 300 ppm, the inhibition efficiency improves to 83.8%. The existence of the DMIH compound in the pitting solution decreases the corrosion rate and, therefore, increases the inhibition efficiency.

The corrosion mechanism of LCS in oxygenated acidic chloride solutions can be summarized according to ref. 35 as follows:

$$Fe + H_2O + Cl^- \rightarrow [FeClOH]_{ads}^- + H^+ + e^- \quad (4)$$

Table 2 Data of WL measurements at 240 minutes for LCS in a 0.5 mol L^{-1} HCl, in the absence and presence of different concentrations of the DMIP compound at different temperatures

Temperature (K)	[DMIH] (ppm)	k (kg m^{-2} s^{-1} × 10^{-9})	θ	IE_w (%)
298	0.00	78.5	—	—
	50	27.9	0.639	63.9 ± 0.2
	100	25.4	0.672	67.2 ± 0.1
	150	22.5	0.709	70.9 ± 0.3
	200	18.7	0.758	75.8 ± 0.1
	250	16.3	0.790	79.0 ± 0.4
	300	12.5	0.838	83.8 ± 0.3
308	0.00	80.00	—	—
	50	27.98	0.600	60.0 ± 0.3
	100	25.41	0.642	64.2 ± 0.4
	150	22.53	0.684	68.4 ± 0.1
	200	18.74	0.705	70.5 ± 0.2
	250	16.32	0.753	75.3 ± 0.2
	300	12.50	0.768	76.8 ± 0.1
318	0.00	83.00	—	—
	50	31.67	0.574	57.4 ± 0.3
	100	28.33	0.590	58.0 ± 0.5
	150	25.00	0.631	63.1 ± 0.1
	200	23.33	0.662	66.2 ± 0.4
	250	19.58	0.687	68.7 ± 0.3
	300	18.33	0.759	75.9 ± 0.2
328	0.00	86.00	—	—
	50	34.58	0.527	52.7 ± 0.1
	100	33.33	0.565	56.5 ± 0.3
	150	30.00	0.599	59.9 ± 0.1
	200	27.50	0.638	63.8 ± 0.4
	250	25.42	0.657	65.7 ± 0.5
	300	19.58	0.720	72.0 ± 0.2

$$[FeClOH]_{ads}^- \leftrightarrow [FeClOH]_{ads} + e^- \text{ (rate determining step)} \quad (5)$$

$$[FeClOH] + H^+ \leftrightarrow Fe^{2+} + Cl^- + H_2O \quad (6)$$

In the presence of oxygen,[34] the reduction reaction is:

$$4H^+ + O_2 + 4e^- \rightarrow 2H_2O \quad (7)$$

- Iron (Fe) reacts with water (H_2O) and chloride ions (Cl^-) to form an intermediate adsorbed molecule ($[FeClOH]_{ads}^-$) and releases a hydrogen ion (H^+) and an electron (e^-) (eqn (4)).
- The intermediate undergoes a slower reaction (rate-determining step) to form ferrous ions (Fe^{2+}), releasing another chloride ion and water molecule (eqn (5) and (6)).
- In the presence of oxygen (O_2) and acidic conditions, the main cathodic reaction involves oxygen consuming four protons (H^+) and four electrons (e^-) to form two water molecules (H_2O) (eqn (7)).

When the organic inhibitor (DMIH) is added to the HCl solution, it forms a thin film on the steel surface and slows down the rate of corrosion. This is the result of a substitution process that occurs on the metal/solution boundary between inhibitor and water molecules. The substitution process is described by eqn (8).[35]

$$xH_2O_{(ads)} + org_{(sol)} \Rightarrow org_{(ads)} + xH_2O_{(sol)} \quad (8)$$

The size ratio, or x, is the number of water molecules that one organic inhibitor molecule displaces. The effectiveness of the inhibitor depends on its shape. Planar molecules offer better surface coverage, leading to stronger protection against corrosion.[35]

3.2.2 Effect of temperature. The corrosion rate and the inhibition efficiency were estimated in the temperature range of 298–328 K. Table 2 shows the obtained results. The corrosion rate in the absence or presence of the synthetic inhibitor increases with increasing temperature. This is because the kinetic motion of the electrolyte (HCl) and hydrogen gas bubbles increases, causing the protective film to desorb from the metal surface and increasing the exposed area of the metal subjected to the HCl solution. By adding DMIH in different concentrations (50–300 ppm) to the blank solution, the dissolution rate significantly decreased. At 298 K and in the presence of 300 ppm of the DMIH compound, the inhibition efficiency was 83.8%. Increasing the temperature to 328 K decreases the inhibition efficiency to 72%. It can be concluded that as the inhibition efficiency decreases with increasing temperature, the adsorption of the DMIH compound on the LCS surface belongs to the physical type.[36]

3.3 Corrosion kinetics

Arrhenius and transition-state equations are used to estimate the activation parameters, such as activation energy (E_a^*), enthalpy change (ΔH_a^*), and entropy change (ΔS_a^*) for the dissolution of LCS in a 0.5 mol L^{-1} HCl solution in the absence and presence of various concentrations of the DMIH inhibitor.[10,36]

$$k = A\exp\left(\frac{-E_a^*}{RT}\right) \quad (9)$$

$$\ln\left(\frac{k}{T}\right) = \left(\ln\left(\frac{R}{Nh}\right) + \left(\frac{\Delta S_a^*}{R}\right)\right) - \frac{\Delta H_a^*}{RT} \quad (10)$$

where k is the rate of corrosion, A is the pre-exponential factor, R is the gas constant, N is the Avogadro's number, T is the absolute temperature, and h is the Planck's constant. Arrhenius plots ($\log k$ *vs.* $1/T$) are shown in Fig. 3 (left) for the LCS immersed in a blank solution in the absence and presence of a variety of DMIH concentrations. The high values (0.99) of the regression coefficient (R^2) reflect the high quality of the obtained results. The slopes and intercepts of the plots give the magnitudes of E_a^* and A, respectively. The inhibiting effect of the DMIH on the corrosion process is confirmed by the higher computed values of E_a^* for inhibited solutions compared to the blank solution (Table 3). The activation energy of the blank solution is 3.5 kJ mol^{-1}. In the presence of 300 ppm of the DMIH compound, the activation energy increases to 16.8 kJ mol^{-1}. The enthalpy and entropy of activation can be calculated from the slopes and intercepts of the transition-state plots ($\log k/T$ *vs.* $1/T$), respectively (Fig. 3 (right)). Their values are shown in Table 3. It is evident from the data in Table 3 that ΔS_a^* values are negative for LCS in the absence and presence of the DMIH compound. This suggests that the activated complex that is formed in the transition state is more ordered at the surface of the LCS.[16,18]

It was also observed from Table 3 and Fig. 3 (right) that the change of ΔH_a^* values is positive for LCS in the absence and presence of various concentrations of the DMIH compound. The endothermic feature of the LCS under study was influenced by this behavior, which can be attributed to the detrimental effect of elevated temperatures on the efficiency of inhibition.[10]

Table 3 Activation parameters for corrosion of LCS in 0.5 mol L^{-1} HCl without and with different concentrations of the DMIH compound

[DMIH] (ppm)	E_a^* (kJ mol^{-1})	ΔH_a^* (kJ mol^{-1})	$-\Delta S_a^*$ (J mol^{-1} K^{-1})	R^2
Blank	3.5	0.9	263	0.99
50	10.6	8.0	251	0.99
100	11.1	8.5	250	0.99
150	12.6	10.0	48	0.99
200	12.9	10.3	47	0.99
250	14.6	12.0	42	0.99
300	16.8	14.2	35	0.99

3.4 Adsorption isotherm

The behavior of a DMIH inhibitor on the LCS surface has been explained by many kinds of adsorption isotherm models, including Langmuir, Temkin, Frumkin, Flory-Huggins, and Freundlich, based on weight loss data.[37] The following equation indicates that the adsorption of the synthesized compound on the LCS surface followed the Langmuir isotherm.

$$\frac{C}{\theta} = \frac{1}{K_{ads}} + C \quad (11)$$

where C is the inhibitor concentration, K_{ads} is the equilibrium constant of the adsorption process, and (θ) is the surface coverage. Fig. 4 shows the plots of C/θ *vs.* C. The figure demonstrates linear relationships with regression coefficients of 0.9999. The slopes of the lines slightly deviate from the value of one due to lateral interactions between adsorbed molecules.[21,22] The equilibrium constant, K_{ads}, is determined from the reciprocal of the intercepts of the lines in Fig. 4. The values of K_{ads} are given in Table 4. The high values of K_{ads} indicate that the adsorbed film is strong and stable.[37] The value of K_{ads} decreases with increasing

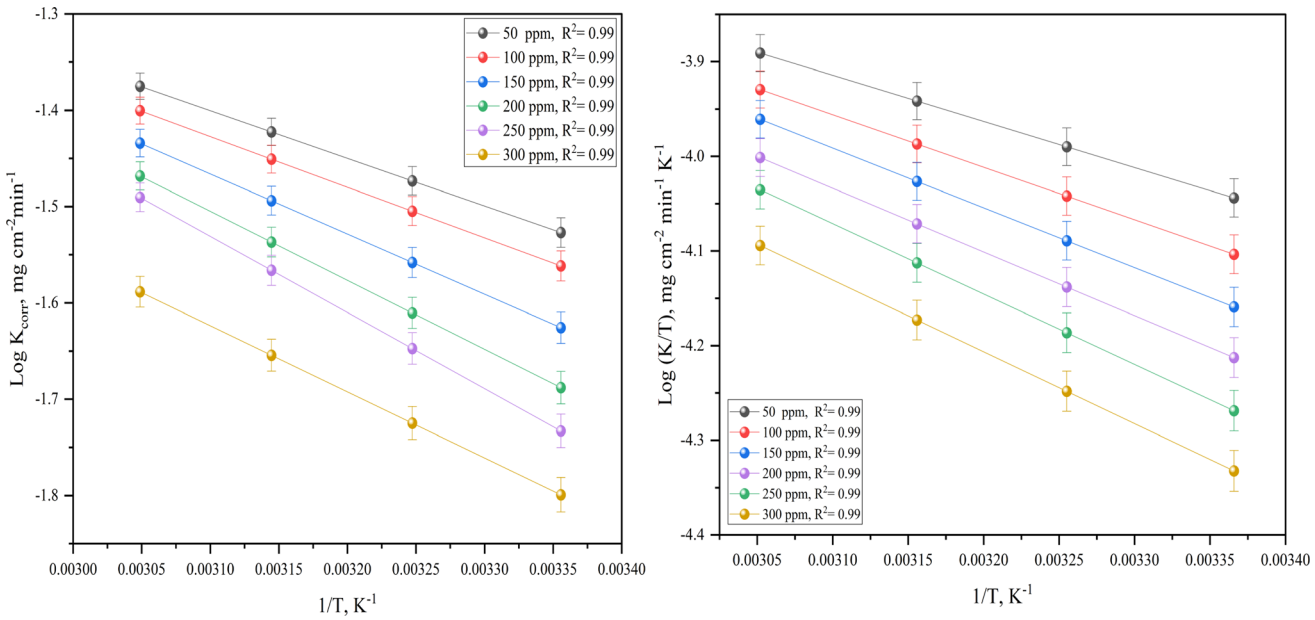

Fig. 3 Arrhenius plots (left) ($\log k$ *vs.* $1/T$) and transition-state plots (right) ($\log k/T$ *vs.* $1/T$) for the corrosion of low-carbon steel in 0.5 mol L^{-1} HCl without and with different concentrations of the DMIH compound.

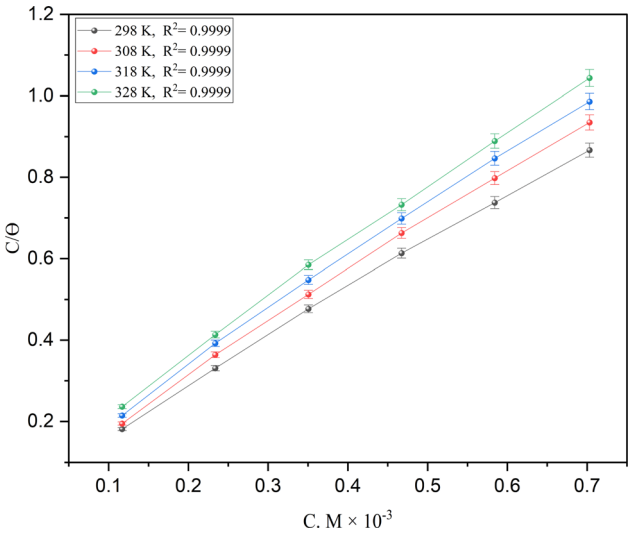

Fig. 4 The Langmuir adsorption isotherms for the DMIH compound on low-carbon steel in 0.5 mol L^{-1} HCl at different temperatures.

temperature until 318 K, then increases at elevated temperature (328 K). Rising temperatures increase the rate of desorption of DMIH molecules from LCS due to the physical nature of the adsorption. At elevated temperatures, the physical adsorption changes to chemical adsorption, and hence the value of K_{ads} increases (Table 3).[26,28] As was previously established, K_{ads} was associated with the standard free energy of adsorption, ΔG°_{ads}, which was calculated from the eqn (12).[38,39]

$$K_{ads} = \exp\left(\frac{-\Delta G^{\circ}_{ads}}{RT}\right) \quad (12)$$

where R is the gas constant, and T is the absolute temperature. Table 4 presents the computed ΔG°_{ads} of the synthesized DMIH compound at different temperatures (298–328 K). The adsorption of the DMIH compound on the LCS surface was spontaneous and stable, based on the negative value of ΔG°_{ads}. Furthermore, chemisorption and physisorption processes have been distinguished in numerous investigations based on ΔG°_{ads} values.[25,26] ΔG°_{ads} with values of -20 kJ mol^{-1} and lower were correlated with an interaction of electrostatic charges between inhibitor molecules and the LCS surface (physisorption), while values of -40 kJ mol^{-1} and higher were associated with electron transfer between the inhibitor molecules and the LCS surface (chemisorption). In the current study, the values of ΔG°_{ads} for the DMIH compound are in the range of -26.8 to -28.5 kJ mol^{-1}. Therefore, the adsorption of the DMIH compound on the LCS surface is a complex mixed form of chemical/physical adsorption, not typical physisorption or chemisorption.[40,41]

3.5 Electrochemical measurements

3.5.1 Open circuit potentials (OCP)–time curves. The open circuit potential (OCP) of the LCS electrode *versus* the SCE was investigated in the absence and presence of various concentrations of the manufactured DMIH inhibitor as a function of exposure time. The OCP–time curves of the LCS in 0.5 mol L^{-1} HCl solution, without and with different doses of the synthetic inhibitor, are shown in Fig. 5a. In the presence of the inhibitor, the LCS electrode's corrosion potential (E_{corr}) changed in a more noble direction until a steady-state potential was attained. The reason for this behavior is that the synthesized inhibitor adheres to the LCS surface, reducing the number of active sites. This implies that the presence of the synthesized inhibitor had a greater impact on the kinetics of the anodic reaction of the LCS in a 0.5 mol L^{-1} HCl solution.[26] It is worth observing that the curves for the LCS in the presence of the inhibitor tend to flatten out over time, whereas the curve for the LCS in the blank solution continues to decrease. This further implies that a protective film is being formed by the inhibitor on the steel's surface.

3.5.2 PDP measurements. The relationship between the overpotential and the logarithmic current density can be shown using a Tafel plot. The Tafel slopes (β_a and β_c), corrosion potential (E_{corr}), and corrosion current density (I_{corr}) can then be calculated using the extrapolation method.[32] The Tafel polarization curves of LCS in a 0.5 mol L^{-1} HCl acid without and with different concentrations of synthesized DMIH compound are shown in Fig. 5b. The steel overpotential–current density line slopes were altered by the addition of DMIH to the corrosive medium. A smaller slope is associated with a greater ability to resist the polarization that occurs at the metallic boundary.[42] As the inhibitor concentration increases from 50 to 300 ppm, the β_a value decreases from 242 to 120 mV dec^{-1}. This indicates that the inhibitor makes the anodic reaction (steel dissolution) more sluggish. A larger potential increase is needed to achieve a tenfold rise in current density because the inhibitor makes it harder for steel atoms to dissolve. This translates to a slower corrosion rate for the LCS. A decreasing β_a with an increasing inhibitor concentration is a positive sign for corrosion inhibition.[43,44] The β_c value decreases from -322 to -50 mV dec^{-1} as the concentration of the inhibitor increases from 50 to 300 ppm. By reducing the anodic reaction rate (steel dissolution), the inhibitor could also decrease the overall demand for electrons. This could lead to a decrease in β_c.

Table 4 Equilibrium constant K_{ads} and standard free energy change ΔG°_{ads} of adsorption of the DMIH compound on low-carbon steel in 0.5 mol L^{-1} HCl at different temperatures

Temperatures (K)	Slope	Intercept $\times 10^{-5}$	$K_{ads} \times 10^{-3}$ (mol^{-1})	$-\Delta G^{\circ}_{ads}$ (kJ mol^{-1})	R^2
298	1.19	77.5	1291.6	27.7	0.9999
308	1.28	90.1	1108.7	26.9	0.9999
318	1.31	91.3	1095.3	26.8	0.9999
328	1.39	45.2	2203.1	28.5	0.9999

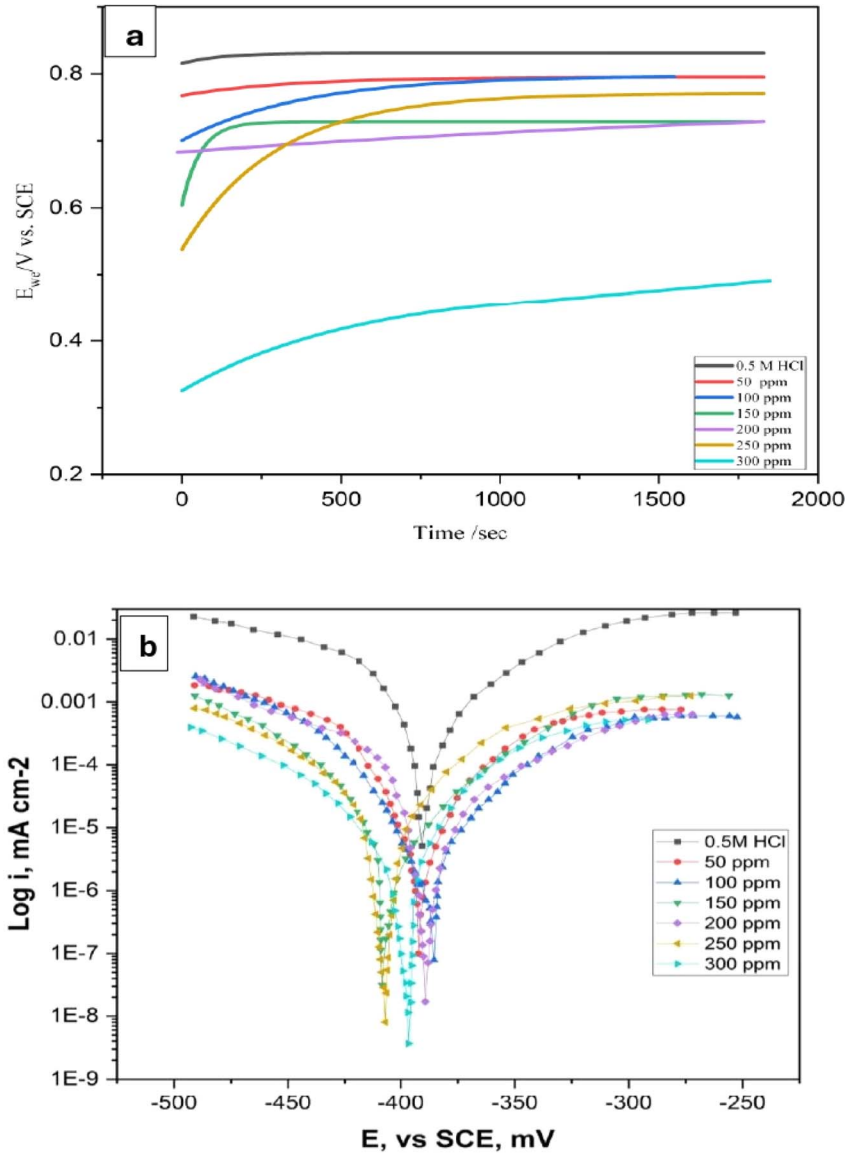

Fig. 5 OCP–time curves (a) and potentiodynamic polarization curves (b) of low-carbon steel in 0.5 mol L^{-1} HCl without and with different concentrations of the DMIH compound at 298 K.

Table 5 Potentiodynamic polarization parameters of low-carbon steel in 0.5 mol L^{-1} HCl without and with different concentrations of the DMIH compound at 298 K

[DMIH] (ppm)	$-E_{corr}$ (mV *vs.* SCE)	β_a (mV dec^{-1})	$-\beta_c$ (mV dec^{-1})	I_{corr} (mA cm^{-2})	θ	IE_p (%)
Blank	391	242	322	1.52	—	—
50	392	235	213	0.55	0.638	63.8 ± 0.1
100	384	220	158	0.50	0.671	67.1 ± 0.4
150	407	210	148	0.45	0.704	70.4 ± 0.2
200	388	185	122	0.38	0.750	75.0 ± 0.3
250	406	140	95	0.25	0.836	83.6 ± 0.1
300	396	120	50	0.17	0.888	88.8 ± 0.1

As the concentration of DMIH increases in corrosive media, the anodic and cathodic branches of the observed polarization curves gradually move toward the lower current density, indicating a decrease in the overall corrosion rate.[35] Increasing the DMIH concentration in solution causes the anodic branch of the polarization curve to shift downward towards lower

current densities. This suggests a decrease in the rate of the anodic reaction. The anodic branch represents the current density associated with iron going into the solution ($Fe \rightarrow Fe^{2+} + 2e^{-}$). A lower current density in this branch signifies a slower rate of steel dissolution, which means a lower corrosion rate for the LCS. The cathodic branch represents the current density

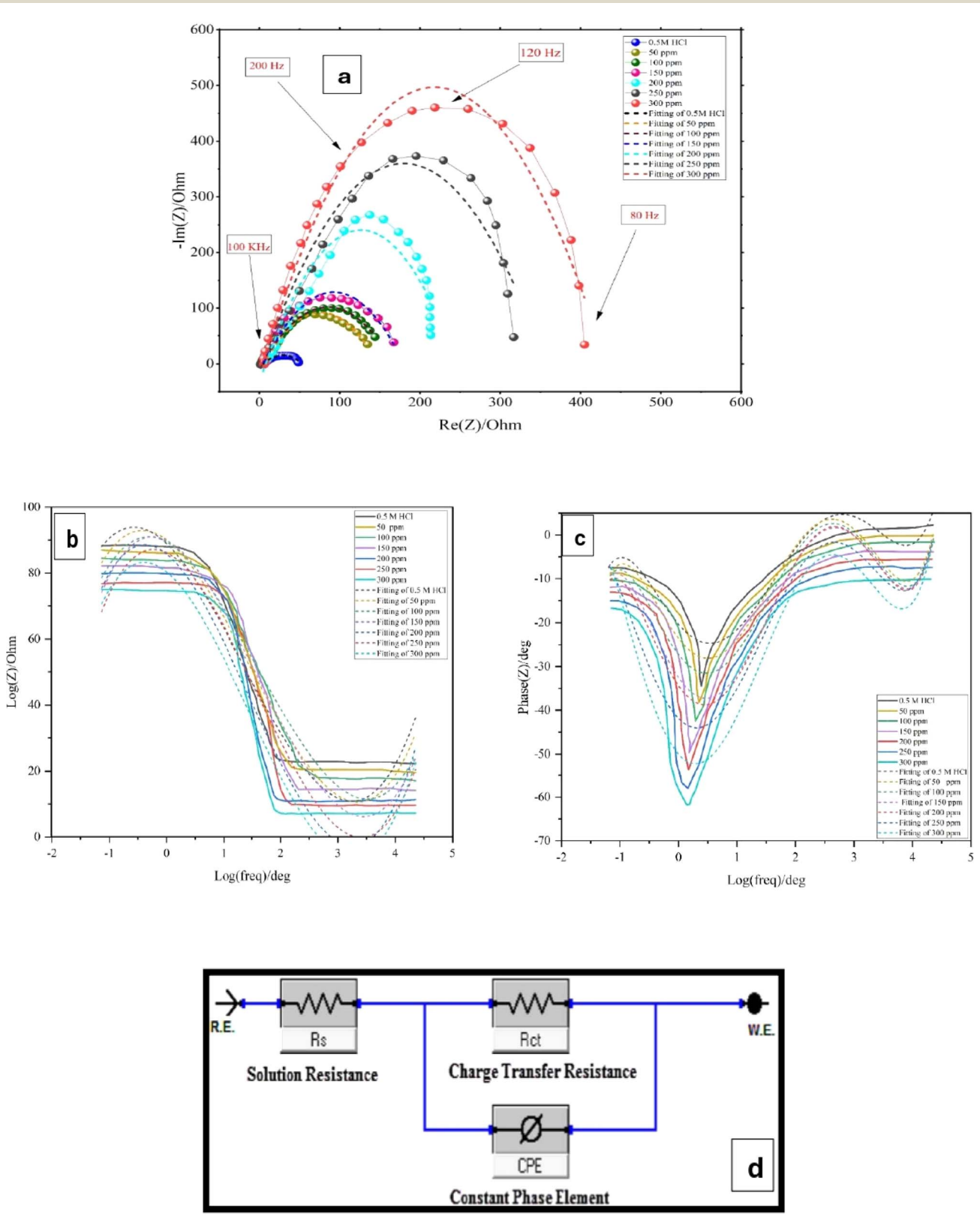

Fig. 6 Nyquist (a) and Bode impedance (b) and phase plots (c) of LCS in 0.5 mol L^{-1} HCl without and with different concentrations of DMIH compound at 298 K and (d) equivalent circuit used to fit the EIS data.

associated with the cathodic reaction (formation of water in oxygenated acidic environments: $4H^+ + O_2 + 4e^- \rightarrow 2H_2O$). While DMIH might not directly target the formation of water, a decrease in the anodic reaction rate (steel dissolution) can indirectly influence the cathodic branch. The overall corrosion process involves the transfer of electrons. A slower rate of steel dissolution (anodic reaction) would mean a lower supply of electrons to the cathode. This leads to a decrease in the current density for the cathodic reaction.[45]

Table 5 shows the electrochemical parameters obtained from Fig. 5b. The inhibition efficiency (IE_p) of the DMIH compound was calculated using eqn (13).

$$IE_p = \frac{i^o_{corr} - i_{corr}}{i^o_{corr}} \times 100 \quad (13)$$

where i^o_{corr} and i_{corr} are the corrosion current densities without and with the DMIH compound, respectively. The corrosion current density (i_{corr}) was calculated by eqn (14).

$$i_{corr} = \beta/R_p \quad (14)$$

where β is a constant correlated with the scientists Stern and Geary, and R_p is the resistance of polarization.[16]

$$\beta = \frac{\beta_a \cdot \beta_c}{2.303(\beta_a + \beta_c)} \quad (15)$$

where β_a and β_c are the anodic and cathodic Tafel slopes, respectively. The type of corrosion inhibitor is identified using the obtained E_{corr}. The inhibitor functions as either a cathodic or anodic type if the E_{corr} value is greater than 85 mV relative to the blank solution and as a mixed type, if the E_{corr} value is less than 85 mV. For the present study, the difference between E_{corr} in the presence of an inhibitor (300 ppm) and in the blank solution is 16 mV (Table 5), indicating that the DMIH compound is a mixed inhibitor.[31] Table 5 displays data revealing a significant decrease in current density upon the addition of the DMIH compound. The efficiency of inhibition improves to 88.8% as the concentration of inhibitor increases to 300 ppm. The Tafel cathodic and anodic constants exhibit a drop in value as the concentration of DMIH increases in the corrosive medium. Adsorption of inhibitor molecules onto the LCS surface may be the cause of these effects.[46] Furthermore, the corrosion potential showed a slight decrease. According to these results, the tested compound functions as a mixed inhibitor.[36]

3.5.3 EIS measurements

3.5.3.1 Effect of inhibitor concentration. Because impedance spectroscopy is a non-destructive technique, it can give information about characteristics across time and ongoing processes like corrosion and other electrochemical reactions.[33] The shape of the impedance diagram can provide mechanistic information. Fig. 6a (Nyquist plot) shows a complex plane impedance diagram ($-\mathrm{Im}(Z)$ *vs.* $\mathrm{Re}(Z)$) of a LCS electrode in a blank solution in the absence and presence of distinct concentrations of the DMIH compound at 298 K. Double-layer capacitance and the time constant of the charge transfer are responsible for the depressed charge transfer semicircle that was seen at high frequencies.[33] It is evident that there is a slight difference between the forms of the impedance graphs for the inhibited and uninhibited LCS. The inhibitor improves the impedance but has no effect on other aspects of the behavior. These findings confirm that the inhibitor has no effect on the electrochemical reactions that cause corrosion, as indicated by the results of polarization experiments. Adsorption on the metal surface is the main mechanism by which the DMIH compound resists corrosion. The Nyquist plot shows multiple semi-circular loops with increasing diameters as the inhibitor concentration increases from 50 to 300 ppm. This suggests that the organic inhibitor increases the charge transfer resistance (R_{ct}), signifying a decrease in the corrosion rate as the inhibitor concentration goes up. The presence of incomplete semi-circles indicates limitations in capturing the entire response at high and low frequencies. This can make the estimation of R_s less accurate. The Bode graphs (Fig. 6b) show that when DMIH exists, the impedance module $|Z|$ is displaced towards greater magnitudes compared to the blank, which is related to the DMIH molecules' adsorption on the LCS surface.[47] Therefore, the LCS corrosion process in an acidic medium was slowed down in its kinetics by the evaluated DMIH.[48]

There is a directly proportionate relationship between $\log Z$ and $\log f$ for Bode graphs in the middle frequency range (Fig. 6b). The slope value is close to -1, while the phase angle value is close to $-75°$ (Fig. 6c). This validates that the capacitive performance at intermediary frequencies is not optimal.[25] It has been stated that when the slope is -1 and the angle of phase is -90 at moderate frequencies, perfect capacitive performance is achieved.[25] Inhibited solutions exhibit greater magnitudes of slope and phase angle compared to uninhibited ones (Fig. 6b and c). This clarifies how well the investigated compound suppresses the breakdown of LCS.

3.5.3.2 Equivalent circuit and impedance parameters. The computer program ZSimpWin was used to analyze the measured impedance data. It was based on the electrical equivalent circuit, shown in Fig. 6d, to compute the impedance variables of the LCS in the corrosive media in the absence and presence of the DMIH compound.[20,22] The equivalent circuit includes the double layer capacitance (C_{dl}) in parallel to the charge transfer resistance (R_{ct}). Both are in series with solution resistance (R_s). Since the resultant capacitive loop is a depressed semi-circle rather than a regular one, one constant phase element (CPE) is replaced for the capacitive element to provide a more precise match.[33] The CPE is a unique element whose phase remains constant regardless of the frequency and whose admittance value depends on the angular frequency (ω). Its impedance and admittance are represented as follows:

$$Y_{CPE} = Y_o(j\omega)^n \quad (16)$$

and

$$Z_{CPE} = \frac{1}{Y_o(j\omega)^n} \quad (17)$$

where Y_o is the magnitude of the CPE, j is the imaginary number ($j = \sqrt{-1}$), α is the phase angle of the CPE, and $n = \alpha/(\pi/2)$. The factor n normally ranges between 0.50 and 1.0.[33] A perfect capacitor is described by the CPE for $n = 1$. α values are typically

Table 6 EIS data of low-carbon steel in 0.5 mol L^{-1} HCl without and with different concentrations of the DMIH compound at 298 K

[DMIH] (ppm)	R_s (Ω cm^2)	R_{ct} (Ω cm^2)	n	$C_{dl} \times 10^{-6}$ (F cm^{-2})	Y_o ($m\Omega^{-1}$ s^n cm^{-2})	θ	$\chi^2 \times 10^{-3}$ (%)	IE_{EIS} (%)
Blank	4.88	48.6	0.84	108	0.180	—	3.42	—
50	5.14	134.7	0.82	38	0.135	0.639	4.15	63.9 ± 0.3
100	4.18	144.0	0.79	30	0.098	0.663	6.32	66.3 ± 0.3
150	5.89	164.6	0.77	22	0.070	0.705	5.04	70.5 ± 0.2
200	4.51	213.3	0.78	19	0.061	0.772	3.68	77.2 ± 0.4
250	4.43	309.6	0.79	14	0.052	0.843	7.55	84.3 ± 0.1
300	5.24	404.8	0.80	11	0.041	0.888	5.48	88.8 ± 0.2

associated with the electrode surface roughness. The higher the surface roughness, the smaller the value of α.[44,45] For our experimental results, a satisfactory match was obtained with this model. The point of intersection between the semicircle and the real axis at high frequency gives R_s. However, the intercept at lower frequencies represents $(R_s + R_{ct})$. Eqn (18) uses the frequency (F_{max}) at which the imaginary component of the impedance is at its maximum to get C_{dl}.

$$C_{dl} = \frac{1}{2\pi} F_{max} R_{ct} \quad (18)$$

The maximum phase angle (θ_{max}) of the impedance, R_{ct}, and C_{dl} were used to assess the inhibitor's efficiency of inhibition. The width of the semicircle increases with the density of the inhibitor's monolayer, leading to a decrease in C_{dl} values and an increase in R_{ct} values (Table 6). It has been established that for $R_s = 0$, θ_{max} for a corrosion interface represented by a straightforward R–C parallel equivalent circuit should be 90°. For real electrode/solution interfaces, depressed semicircles are often observed, and this has been attributed to the roughness of the electrode surface. Hydrochloric acid solutions cause the steel to corrode, which boosts the electrode surface's roughness (please refer to the SEM image in Fig. 7b, Section 3.6) and lowers the value of θ_{max}.

Eqn (19) was used to determine the IE_{EIS} of the DMIH at different concentrations at 298 K based on the R_{ct} values.[33]

$$IE_{EIS} = \frac{R_{ct} - R_{ct}^{o}}{R_{ct}} \times 100 \quad (19)$$

where R_{ct}^{o} and R_{ct} are the charge-transfer resistances for the blank and inhibited solutions, respectively. The data obtained from EIS measurements for the dissolution of the LCS in the blank solution without and with different DMIH concentrations at 298 K are summarized in Table 6. It is apparent that as the concentration of the DMIH compound increases, the inhibition efficiency and R_{ct} increase, but C_{dl} decreases. The observed increase in R_{ct} and decrease in C_{dl} with increasing inhibitor concentrations suggest that the inhibitor molecules affect the corrosion process through a combined mechanism. This behavior is characteristic of mixed inhibitors. The previous findings confirm inhibitor adsorption and the formation of a protective film on the LCS surface. The values of n are close to 0.8, suggesting a non-ideal capacitance at the electrode/electrolyte interface, with minimal change upon inhibitor addition. The value of Y_o decreases with increasing inhibitor concentration. This might indicate a decrease in surface roughness or inhomogeneity with inhibitor adsorption.[21] A small value of the Chi-square parameter (χ^2) suggests a good fit of experimental data.

Potentiodynamic polarization and EIS techniques predict different inhibition efficiencies, which should be noted. In fact, differences in the electrode material's surface condition are responsible for the inconsistencies between the two methods.[26]

3.6 SEM and AFM analysis

SEM examination is a useful method for investigating the surface morphology of LCS after it has been immersed in corrosive media. This method is particularly useful for describing the formation of

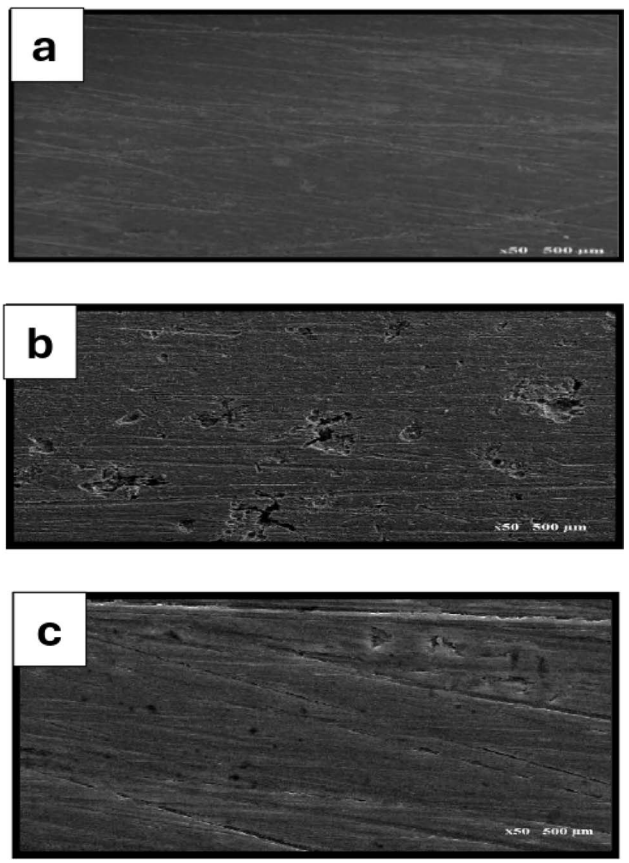

Fig. 7 SEM micrographs of polished LCS (a) and LCS after 48 hours of immersion in a 0.5 mol L^{-1} HCl without (b) and with (c) 300 ppm of the DMIH compound at 298 K.

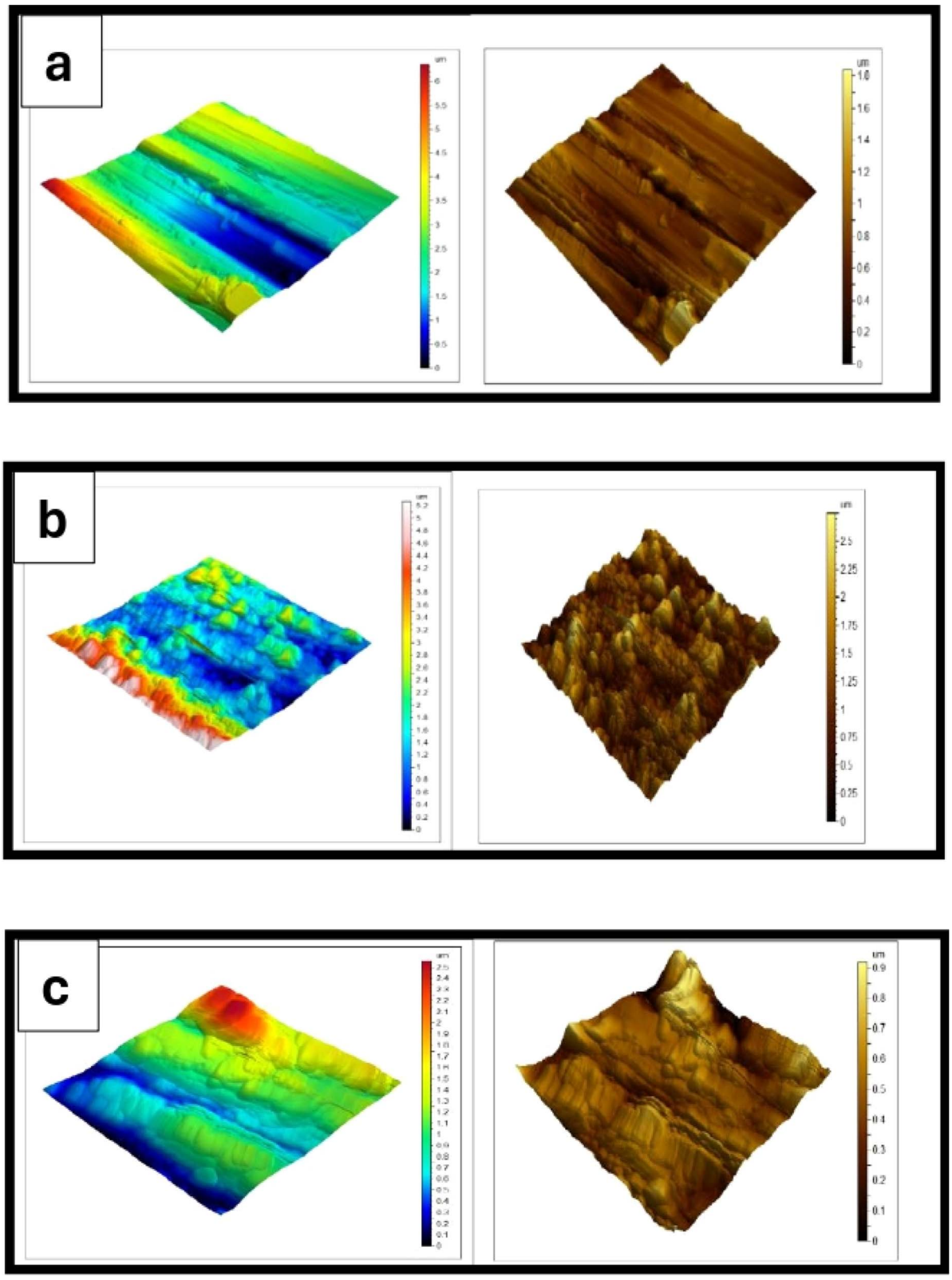

Fig. 8 AFM three-dimensional pictures of LCS (a), LCS after 48 h immersion in a 0.5 mol L^{-1} HCl without (b) and with (c) 300 ppm of DMIH compound at 298 K.

a surface-protective organic layer that permits a high degree of inhibition resistance.[5] SEM micrographs of polished LCS and LCS after 48 hours of immersion in a blank solution in the absence and presence of 300 ppm of the DMIH compound at 298 K are shown in Fig. 7. When the DMIH is not present, the pitting actions of Cl^- and H_3O^+ ions cause localized corrosion on the LCS surface

(Fig. 7b).[33] However, the rate of corrosion is suppressed when the DMIH inhibitor is present, as seen by the reduction in localized corrosion areas. The inhibitor forms an adsorbed film on the LCS surface (Fig. 7c). Measurements of inhibition efficiency using chemical and electrochemical techniques demonstrate the film's protective properties.

To examine the surface features at microscales, AFM is used. It is a magnificent and innovative instrument to investigate how the inhibitor affects the corrosion reaction at the LCS solution interface. The AFM morphologies of polished LCS and LCS in a blank solution in the absence and presence of 300 ppm of the DMIH compound are shown in Fig. 8. When the LCS is exposed to a blank solution, the metal surface is noticeably more deteriorated than when the organic compound is present (Fig. 8b and c). Table 7 provides all height parameters. These are the maximum peak height (S_p), maximum pit height (S_v), maximum height (S_z), arithmetic mean height (S_a), and root-mean square height (S_q).[49] In accordance with ISO 25178,[50] they are calculated in micrometer units. The expression (control) in Table 7 refers to the baseline or untreated condition for the AFM parameters of LCS. It serves as a reference point for comparison with the other substances (0.5 mol L^{-1} HCl and DMIH). The values for all parameters in the 0.5 mol L^{-1} HCl solution are significantly higher than those in the control, indicating that the hydrochloric acid solution increased the roughness of the steel surface. The average roughness (S_a) of LCS in a 0.5 mol L^{-1} HCl solution is 0.254 μm, and the maximum height (S_z) is 9.60 μm. However, in the presence of the DMIH compound, the values of surface parameters are much lower than in the blank solution due to the adsorption of the DMIH molecules at the LCS surface and the formation of a protective film.[18] The average roughness and the maximum height decrease to 0.066 and 1.91 μm, respectively. Consequently, the results of the chemical and electrochemical analyses indicating that the DMIH compound is an effective LCS inhibitor in HCl solutions are supported by SEM and AFM analyses of the LCS surface.

3.7 Quantum chemical calculations

3.7.1 DFT results. The inhibiting impact of the DMIH compound on LCS in a 0.5 mol L^{-1} HCl solution was explained by quantum chemistry investigations employing the DFT method.[51] DFT-based quantum chemistry investigations were utilized to provide an explanation for DMIH's inhibitory effect on LCS in 0.5 mol L^{-1} HCl.[45] Calculating different quantum chemical properties like dipole moment, energy gap (ΔE), HOMO, and LUMO energy can be done with the DFT method. Fig. 9 shows the optimized geometry of the HOMO and LUMO frontier molecules, the optimized DMIH structure, and the molecular electrostatic potentials (MEP) of the DMIH inhibitor. The different quantum chemical parameters for the DMIH are listed in Table 8. The values of the parameters are obtained based on the following relationships:[22,52]

$$\Delta E = E_{LUMO} - E_{HOMO} \quad (20)$$

$$I = -E_{HOMO} \quad (21)$$

$$A = -E_{LUMO} \quad (22)$$

$$\mu = -\chi \quad (23)$$

$$\mu = \frac{(E_{HOMO} + E_{LUMO})}{2} \quad (24)$$

$$\eta = \frac{(E_{LUMO} - E_{HOMO})}{2} \quad (25)$$

$$\sigma = 1/\eta \quad (26)$$

$$\Delta N_{max} = \frac{-\mu}{\eta} \quad (27)$$

$$\omega = \frac{\mu^2}{2\eta} \quad (28)$$

The calculations showed that the investigated organic compound's geometrical structures are nearly planned, as Fig. 9 illustrates. The relationship between HOMO and LUMO levels has been found to affect chemical reactivity.[53] The calculated HOMO and LUMO energies are −0.229 and −0.037, respectively, indicating that the DMIH compound can function as an electron donor and enhance the formation of a protective layer on the LCS surface.[54] DMIH may effectively suppress the corrosion process, as demonstrated by its computed ΔE value of 0.192 (Table 8). An increase in inhibiting efficiency has been reported as ΔE decreases.[36] The HOMO electron density distribution indicates that the DMIH molecule can transfer electrons to the steel metal *via* the π-orbitals of the benzene ring, O of the methoxy and carbonyl groups, and N of the $NHNH_2$ groups (Fig. 9). The distribution of the LUMO electron density indicates that the entire structure of the DMIH molecule can accept electrons from the steel metal. The electron density maps of the DMIH molecule are displayed in Fig. 9. Based on the mapping of the synthetic organic compound's molecular electrostatic potential (MEP), the nucleophilic centers (the red areas) for adsorption at the steel surface are the π-orbitals, the O atoms of the methoxy and carbonyl groups, and the N atoms of the $NHNH_2$ groups. This enhances the potential of the adsorption process and develops a shielding film on the metal surface that improves the efficiency of inhibition. The molecule's adsorption at the steel surface is enhanced by the electron density, which is distributed throughout the whole molecule. The blue areas in the DMIH molecule can function as electrophiles and accept electrons from 3d-filled orbitals of steel.[10]

Uneven charge distribution among the atoms in the DMIH molecule causes the dipole moment. According to Table 8, the

Table 7 AFM parameters of low-carbon steel in the blank solution in the absence and presence of 300 ppm of the DMIH compound at 298 K

Substance	S_a (μm)	S_q (μm)	S_p (μm)	S_v (μm)	S_z (μm)
Control	0.045	0.062	0.234	0.436	0.670
0.5 mol L^{-1} HCl	0.254	0.351	6.04	3.56	9.60
DMIH	0.066	0.114	0.488	1.43	1.91

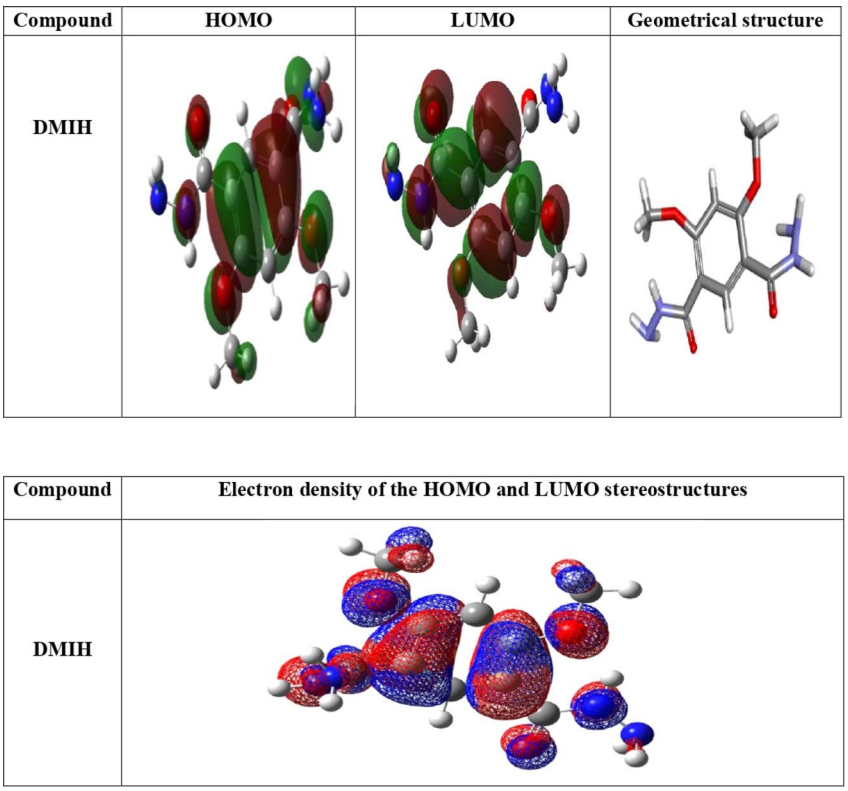

Fig. 9 Geometrical structure, charge density distribution of HOMO and LUMO levels, and electron density plots of the molecular electrostatic potentials (MEP) of the DMIH compound.

dipole moment of the DMIH compound is 8.210 debye. The low value facilitates the accumulation of inhibitor molecules on the steel surface, thereby enhancing the DMIH compound's ability to adsorb.[55] The dipole moment of the DMIH molecule is higher than that of water (1.88 debye), suggesting a strong dipole–dipole interaction between the DMIH molecule and the steel metal. Therefore, water molecules are effectively displaced by DMIH molecules, and the latter are physically adsorbed onto the steel surface.[4] The lower hardness value (0.096) indicates that the DMIH compound is readily absorbed at the steel surface.[5] Another indication that DMIH is an effective corrosion inhibitor is its high global softness value (10.410).[26] If the ionization potential is small, the molecules are more reactive. When it is large, the molecules are more stable.[6] Table 8 showed that DMIH has a good inhibitory efficiency due to its small ionization potential value of 0.229. The electronegativity (χ) of DMIH is low (0.133), suggesting that the transfer of electrons occurs from inhibitor molecules to steel atoms until the system's chemical potentials are equal.[26] Electrophilicity (ω) enables the evaluation of a chemical system's overall electrophilic character.[56] According to the literature, the effective nucleophile and electrophile have lower and greater values of ω, respectively.[57] The more prominent nucleophilic character of the DMIH molecule is indicated by the reported ω value (0.092) in Table 8. For the DMIH compound, the computed ΔN_{max} is 1.385. This indicates the remarkable ability of the DMIH compound to transfer electrons to steel atoms through coordination bonds, resulting in the formation of an effective protective film that hinders metal corrosion.[58] Table 8 shows that the synthesized DMIH compound has a large molar volume (139.15 $cm^3\ mol^{-1}$). This increases the surface contact between the molecules of the inhibitor and the steel surface, which enhances the inhibitor's inhibitory efficiency. Considering the forementioned results and according to the hard and soft acids and bases (HSAB) theory, steel metal can be regarded as a soft acid and the DMIH compound as a soft base.[59]

Table 8 The calculated quantum chemical parameters, obtained from DFT theory

Parameter (au)	Value
Energy of the highest occupied molecular orbital (E_{HOMO})	−0.229
Energy of the lowest unoccupied molecular orbital (E_{LUMO})	−0.037
Energy gap (ΔE)	0.192
Dipole moment (Debye)	8.210
Chemical hardness (η)	0.096
Chemical softness (σ)	10.410
Chemical potential (μ)	−0.133
Electronegativity (χ)	0.133
Electron affinity (A)	0.037
Ionization potential (I)	0.229
Electrophilicity index (ω)	0.092
Maximum charge transfer index (ΔN_{max})	1.385
Total energy (E_t)	−909.39
Volume ($cm^3\ mol^{-1}$)	139.15

3.7.2 Monte Carlo simulations. Monte Carlo (MC) simulations were used to investigate the preferred adsorption

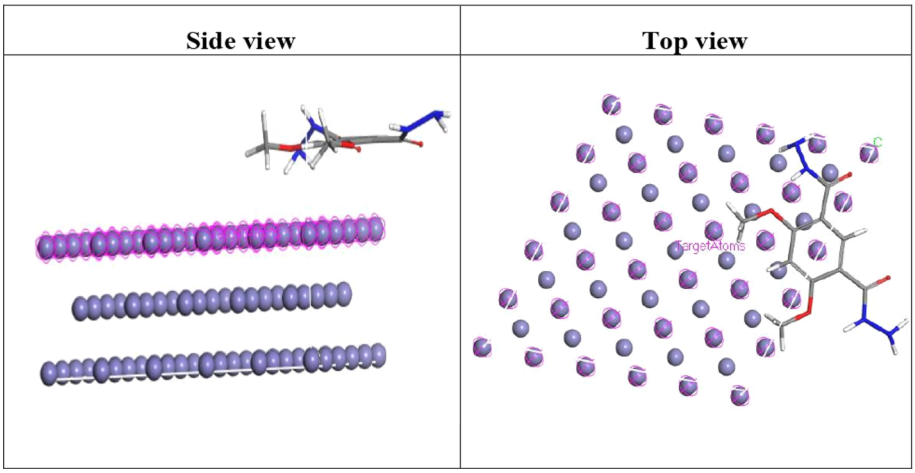

Fig. 10 Side view and top view of the adsorption of the investigated DMIH inhibitor on the LCS surface.

configurations of the DMIH compound on sites of adsorption of the periodic structure of Fe(110). The Fe(110) face was chosen because it has a high surface energy compared to other iron faces, making it more stable and less prone to reconstruction or rearrangement of surface atoms.[60] To find adsorption sites, MC investigated potential substrate-adsorbate configurations using a simulated annealing technique.[61] To prevent interference between periodic unit cells, MC was conducted in a periodic slab model box of super unit cells with a vacuum layer of 30 Å. A supercell of a Fe(110) surface with 9 atomic layers was covered by a single molecular inhibitor. As illustrated in Fig. 10a and b, MC simulation provides us with a clear picture of the orientation and interactions between the synthesized compound and the steel surface. To maximize contact and increase surface coverage, the DMIH is arranged horizontally and parallel to the Fe crystal (110) surface. This results in higher adsorption energy (Table 9) and implies a higher inhibitory efficiency.[55]

Table 9 displays the computed adsorption, deformation, and rigid adsorption energies. Eqn (29) is used to get the adsorption energy, E_{ads}.

$$E_{ads} = E_{Fe-inh} - (E_{inh} - E_{Fe}) \quad (29)$$

where E_{Fe} and E_{inh} stand for the total energies of the steel surface and the inhibitor, respectively. It is assumed that the surface energy of Fe(110) is zero.[62] The energy evolved or absorbed during the adsorption process of the relaxed inhibitor molecule on the steel surface is known as the adsorption energy. It is the sum of the inhibitor molecule's deformation and rigid adsorption energies. The energy generated or absorbed during the unrelaxed inhibitor molecule's adsorption on the steel surface is the rigid adsorption energy. The energy evolved when the adsorbed molecule relaxed is known as the deformation energy. It is clear from Table 9 that E_{ads} has a significant negative value (−1476.59 kJ mol^{-1}). This indicates that the tested compound can substitute corrosive ions and water molecules to create a barrier film that protects the steel surface from the corrosive medium.[55]

3.8 Mechanism of inhibition

The experimental findings indicated that DMIH molecules significantly reduced LCS corrosion in a 0.5 mol L^{-1} HCl electrolyte. To comprehend the method of inhibition, one can utilize the DMIH's structure and adsorption process. As illustrated in Fig. 9, the DMIH structure contains carbonyl, hydrazine and methoxy groups, and π-electrons. DMIH molecules can therefore adsorb on the metal surface.[63,64]

The capability of an inhibitor to adsorb depends on a variety of factors, including its molecular size, chemical structure, the kind of metal and its charged surface, and charge distribution throughout the inhibitor molecule. Two types of adsorptions, chemisorption and physisorption, were considered. The chemisorption mechanism permits the neutral molecules of the DMIH to be adsorbed on the surface of LCS by pushing H_2O molecules away from the LCS surface and sharing electrons between O and N in the DMIH compound and LCS. Additionally, the metal surface does not just passively accept electrons. In return, some electron density from the filled d-orbitals of the metal can flow back into the π-system of the aromatic ring (retrodonation). This "back-donation" strengthens the overall interaction.[65]

It is commonly recognized that the LCS surface has a positive charge in acidic media.[66] Hence, the protonated DMIH molecules find it difficult to get too close to the positively charged

Table 9 The descriptors calculated by the Monte Carlo simulation for the adsorption of the DMIH compound on the steel surface

Total energy (kJ mol^{-1})	Adsorption energy (kJ mol^{-1})	Rigid adsorption energy (kJ mol^{-1})	Deformation energy (kJ mol^{-1})
−414.74	−1476.59	−905.60	−570.99

Table 10 Comparison between the tested DMIH compound and other inhibitors in the literature

Compound name	IE (%)	Reference
• α-Aminophosphonate	92.4	5
• (*N*,*N*′*E*,*N*,*N*′*E*)-*N*,*N*′-(Thiophene-2,5-diylbis(methanylylidene))bis(1*H*-benzo[*d*]imidazole-2-amine)	96.0	10
• Dimethyl-4,6-dihydroxyisophthalate	79.9	22
• Succinic acid	97.5	33
• 4,6-Dihydroxyisophthalaohydrazide	86.2	20
• 4(*p*-Tolyldiazenyl)-2-((*E*)-(*p*-tolylimino)methyl)phenol	55.0	67
• 3-(2-((4-Hydroxybenzylidene)amino)thiazole-4-yl)-2*H*-chromen-2-one	52.9	68
• *N*-(Pyridine-4-ymethylene)-3,4-dihydropyridine-4-amine	88.0	69
• *N*-(4-*N*,*N*-Dimethylaminobenzal)-*p*-anisidine	80.6	70
• *N*-(4-*N*,*N*-Dimethylaminobenzal)-p-toluidine	79.1	70
• *N*-(4-*N*,*N*-Dimethylaminobenzal)-2,4-dinitroaniline	75.9	70
• 4,6-Dimethoxyisophthalohydrazide (DMIH)	83.8	This work

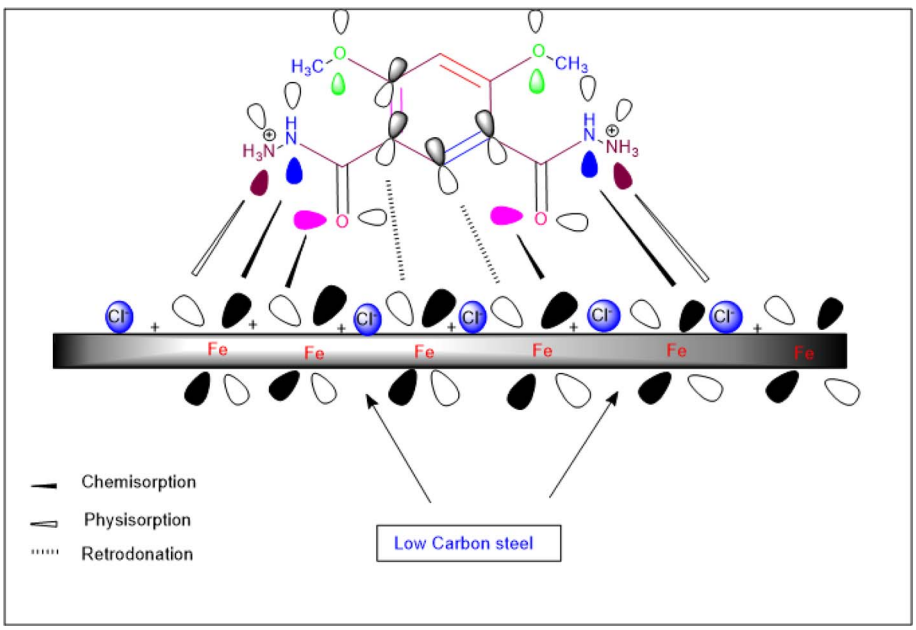

Fig. 11 Schematic figure of LCS corrosion inhibition in a 0.5 mol L^{-1} HCl solution in the presence of the DMIH compound.

LCS surface (H_3O^+/metal contact) because of the electrostatic repulsion. Cl^- ions have the potential to produce additional negative charges close to the interface because they are less hydrated than other ions. Therefore, they enable the protonated DMIH compound to adsorb on the negatively charged LCS surface through electrostatic interactions or physisorption. Fig. 11 shows the inhibition mechanism.

3.9 A comparison of DMIH's inhibitory effectiveness against different organic inhibitors reported in the literature for LCS corrosion

Table 10 displays results from a comparison of the inhibition efficiency established in this study with that of other reported organic inhibitors. The investigation's results were compared favorably with several types of organic inhibitors that are employed to protect LCS. These findings show that the DMIH compound is a good inhibitor.

4. Conclusions and future prospects

In the current investigation, a new resorcinol derivative, namely 4,6-dimethoxyisophthalohydrazide (DMIH), is synthesized and characterized by ^{1}H-NMR spectroscopy. The inhibiting performance of the DMIH compound towards the corrosion of low-carbon steel in a 0.5 mol L^{-1} HCl solution was evaluated. The effectiveness of the inhibitor was examined by chemical and electrochemical methods. The steel morphology was examined by SEM and AFM techniques. The DMIH compound significantly decreased the rate of dissolution of LCS in HCl solution by adsorption. MC and DFT simulations were used to confirm the adsorption of the DMIH compound on the steel surface.

The DMIH compound significantly reduces the corrosion of LCS in a 0.5 mol L^{-1} HCl solution. The highest percentage of inhibition (83.8%) was obtained by 300 ppm of the DMIH compound at 298 K. The IE decreased to 72% as the

temperature increased to 328 K. The anticorrosion performance of the LCS was attributed to the adsorbed DMIH inhibitory film, as confirmed by SEM and AFM analyses. The adsorption of the DMIH compound is categorized using the Langmuir adsorption isotherm. Both chemisorption and physisorption participate in the adsorption of the DMIH compound on LCS. According to the polarization measurements, the DMIH compound is a mixed inhibitor. The potentiodynamic polarization, EIS, and weight loss methods all agreed well with one another. The adsorption of the DMIH compound on LCS through the interaction of O and N atoms is the main factor influencing the rate of LCS specimen degradation in acidic electrolytes. According to different quantum chemical parameters and the hard and soft acids and bases (HSAB) theory, LCS metal can be regarded as a soft acid and DMIH compound as a soft base. The ability of the DMIH compound to form a barrier film that protects the steel surface from the corrosive solution is evidenced by its highly negative adsorption energy (-1476.59 kJ mol^{-1}).

Soon, we will try to prepare new environmentally friendly organic inhibitors derived from the resorcinol compound to protect low-carbon steel from corrosion and degradation in oil and gas fields and achieve high inhibition efficiency. The work will be based on chemical, electrochemical, and theoretical aspects.

Data availability

Data will be made available on request.

Author contributions

M. M. K.: conceptualization, methodology, data curation, writing – original draft preparation & editing. M. A. G.: investigation, funding acquisition & supervision. S. M. R.: data curation, software & methodology. M. A. M.: investigation, methodology, software & validation. S. A. M.: data curation, visualization & software. K. M. H. M.: writing – review & editing. H. E. I.: investigation & validation.

Conflicts of interest

The authors declare no conflict of interest.

Acknowledgements

The authors would like to express their sincere gratitude to the Researchers Supporting Program, Project Number (RSP-2024R518), King Saud University, Riyadh, Saudi Arabia.

References

1 B. A. Shaw and R. G. Kelly, *Electrochem. Soc. Interface*, 2006, **15**(1), 24–26.
2 F. Bentiss, M. Traisnel and M. Lagrenee, *Corros. Sci.*, 2000, **42**(1), 127–146.
3 D. D. Pradnya, B. P. Chetan, S. A. Madhavi and P. M. More, *Vietnam J. Chem.*, 2023, **61**(1), 15–42.
4 N. Kedimar, P. Rao and A. R. Suma, *J. Appl. Electrochem.*, 2023, **53**, 1473–1489.
5 M. A. Deyab, M. M. Abdeen, M. Hussien, I. E. El-Sayed, A. Galhoum, O. A. A. El-Shamy and M. Abd Elfattah, *Molecules*, 2023, **28**, 4962, DOI: **10.3390/molecules28134962**.
6 A. Nasser, N. M. EL Basiony, M. A. Migahed, H. M. Abd-El-Bary and T. A. Mohamed, *Egypt. J. Chem.*, 2022, **65**(SI:13B), 845–867.
7 K. R. Ansari, D. S. Chauhan, A. Singh, V. S. Saji and M. A. Quraishi, *Corrosion Inhibitors in the Oil and Gas Industry*, Wiley-VCH Verlag GmbH & Co. KGaA, 2020, pp. 151–176.
8 M. A. Migahed, M. M. El-Rabiei, H. Nady, H. M. Gomaa and E. G. Zaki, *J. Bio- Tribo-Corros.*, 2017, **3**, 22, DOI: **10.1007/s40735-017-0080-5**.
9 M. M. El-Naggar, *Corros. Sci.*, 2007, **49**, 2226–2236, DOI: **10.1016/j.corsci.2006.10.039**.
10 S. S. Al-Najjar and A. Y. Al-Baitai, *Phys. Chem. Res.*, 2022, **10**(2), 179–194.
11 F. Arjmand, J. Wang and L. Zhang, *J. Mater. Eng. Perform.*, 2016, **25**(3), 1–12, DOI: **10.1007/s11665-016-1903-0**.
12 M. Azaroual, *J. Mol. Liq.*, 2016, **220**, 549–557.
13 R. Farahmand, B. Sohrabi and A. Gha, *Corros. Sci.*, 2018, **136**, 393–401, DOI: **10.1016/j.corsci.2018.03.030**.
14 D. N. Nam, P. V. Hien, N. T. Hoai and V. T. T. Thu, *J. Taiwan Inst. Chem. Eng.*, 2018, **91**, 556–569.
15 S. K. Ahmed, W. B. Ali and A. A. Khadom, *Int. J. Ind. Chem.*, 2019, **10**, 159–173.
16 A. Khadom, H. Liu, C. Fu, J. Wang, N. A. Fadhil and H. B. Mahood, *J. Mol. Liq.*, 2019, **276**, 503–518.
17 H. B. Mahood, A. H. Sayer, A. H. Mekky and A. A. Khadom, *Chem. Afr.*, 2020, **3**, 263–276.
18 S. K. Ahmed, W. B. Ali, A. A. Khadom and J. Bio, *Tribocorrosion*, 2019, **5**, 15, DOI: **10.1007/s40735-018-0209-1**.
19 S. Abd El Wanees, M. M. Kamel, M. Ibrahim, S. M. Rashwan, Y. Atef and M. G. Abd Elsadek, *J. Umm Al-Qura Univ. Appl. Sci.*, 2024, **10**, 107–119.
20 M. M. Kamel, M. A. A. Mahmoud, S. M. Rashwan, S. A. Elmekawy, H. E. Ibrahim and M. K. Awad, *Adv. Environ. Life Sci.*, 2022, **2**, 1–17.
21 A. S. Fouda, S. M. Rashwan, M. M. Kamel, A. H. M. Gad and K. Shalabi, *Int. J. Corros. Scale Inhib.*, 2021, **10**(4), 1407–1427.
22 M. M Kamel, S. M. Rashwan, M. A. A. Mahmoud, S. A. A. El-Mekawy, M. K. Awad and H. E. Ibrahim, *ACS Omega*, 2022, **7**(21), 17609–17619, DOI: **10.1021/acsomega.2c00153**.
23 S. Abd El-Wanees, M. M. Kamel, S. M. Rashwan, Y. Atef and M. G. Abd El Sadek, *Desalin. Water Treat.*, 2022, **248**, 28–38.
24 M. A. Migahed, S. M. Rashwan, M. M. Kamel and R. E. Habib, *Cogent Eng.*, 2017, **4**, 1366255.
25 M. Kamel, M. Hegazy, S. Rashwan and M. El Kotb, *Chin. J. Chem. Eng.*, 2021, **34**, 125–133.
26 M. A. Hegazy, S. M. Rashwan, S. Meleek and M. M. Kamel, *Mater. Chem. Phys.*, 2021, **267**, 124697.
27 M. Kamel, A. A. Fouda, S. Rashwan and O. M. Catrina, *Int. J. Environ. Sci.*, 2022, **26**(1), 19–31, DOI: **10.21608/cat.2022.277040**.

28 M. M. Kamel, A. A. S. Fouda, S. M. Rashwan and O. Abdelkader, *Green Chem. Lett. Rev.*, 2021, **14**(4), 598–609.
29 *Designation: G 1–03; Standard Practice for Preparing, Cleaning, and Evaluating Corrosion Test Specimens*, ASTM International, West Conshohocken, PA, USA, 1990, pp. 19428–22959.
30 *ASTM G59-97; Standard Test Method for Conducting Potentiodynamic Polarization Resistance Measurements*, ASTM International, West Conshohocken, PA, USA, 2014, pp. 1–4.
31 *ASTM G106-89; Standard Practice for Verification of Algorithm and Equipment for Electrochemical Impedance Measurements*, ASTM International, West Conshohocken, PA, USA, 1999, pp. 1–11.
32 *ASTM G16-13; Standard Guide for Applying Statistics to Analysis of Corrosion Data*, ASTM International, West Conshohocken, PA, USA, 2019, pp. 1–14.
33 M. A. Amin, S. S. Abd El-Rehim, E. E. F. El-Sherbini and R. S. Bayoumi, *Electrochim. Acta*, 2007, **52**, 3588–3600.
34 R. A. Alsaiari, M. M. Kamel and M. M. Mohamed, *Molecules*, 2024, **29**, 1157, DOI: **10.3390/molecules29051157**.
35 L. Chen, D. Lu and Y. Zhang, *Materials*, 2022, **15**, 2023, DOI: **10.3390/ma15062023**.
36 B. M. El-Gendya, S. T. Atwaa, A. A. Ahmeda and A. Y. El-Etrea, *Prot. Met. Phys. Chem. Surf.*, 2019, **55**(1), 179–186, DOI: **10.1134/S2070205119010106**.
37 I. Abdelfattah, W. Abdelwahab and A. El-Shamy, *Egypt. J. Chem.*, 2022, **65**(2), 687–694.
38 H. M. A. El-Lateef, V. Abbasov, L. Aliyeva, E. Qasimov and I. Ismayilov, *Mater. Chem. Phys.*, 2013, **142**, 502–512.
39 L. H. Abdel-Rahman, A. M. Abu-Dief, M. Abd-El Sayed and M. M. Zikry, *J. Chem. Mater. Res.*, 2016, **8**, 8–22.
40 H. Fan, S. Li, Z. Zhao, H. Wang, Z. Shi and L. Zhang, *Corros. Sci.*, 2011, **53**, 4273–4281.
41 A. Singh, S. Mohapatra and B. Pani, *J. Ind. Eng. Chem.*, 2016, **33**, 288–297.
42 G. G. Sánchez, O. O. Xometl, P. A. Lozada, N. V. Likhanova, I. V. Lijanova, J. A. Morales, V. D. Jiménez and J. L. Rodríguez, *Int. J. Mol. Sci.*, 2023, **24**, 6291, DOI: **10.3390/ijms24076291**.
43 V. S. Sastri, *Corrosion Inhibitors: Principles and Applications*, John Wiley & Sons, 1998.
44 F. Mansfeld, *Electrochemical Methods of Corrosion Testing*, book chapter, 2003, DOI: **10.31399/asm.hb.v13a.a0003644**.
45 S. About, *Green Inhibitors to Reduce the Corrosion Damage*, 2020, DOI: **10.5772/intechopen.91481**.
46 F. Bentiss, M. Lebrini and M. Lagrenée, *Corros. Sci.*, 2005, **47**(12), 2915–2931.
47 J. Porcayo-Calderon, M. Casales-Diaz, L. M. Rivera-Grau, D. M. Ortega-Toledo, J. A. Ascencio-Gutierrez and L. Martinez-Gomez, *J. Chem.*, 2014, **2014**, 940579.
48 P. Arellanes-Lozada, V. Díaz-Jiménez, H. Hernández-Cocoletzi, N. Nava, O. Olivares-Xometl and N. V. Likhanova, *Corros. Sci.*, 2020, **175**, 108888.
49 A. J. Jawad, *AFM Handbook; Theoretical Principles and Experimental Parameters*, Scholars Press, 2020, ISBN: 978-613-8-940616.
50 Introduction to surface roughness measurement, International Organization for Standardization ISO 25178, **https://sernia.ru/upload/pdf_files/Introductiontosurfaceroughnessmeasurement.pdf**.
51 A. Singh, K. R. Ansari, M. A. Quraishi and P. Banerjee, *J. Mol. Liq.*, 2021, **323**, 114608–114618, DOI: **10.1016/j.molliq.2020.114608**.
52 A. A. Khadom and A. A. Mahmmod, *Results Eng.*, 2022, **16**, 100741, DOI: **10.1016/j.rineng.2022.100741**.
53 D. Q. Zhang, L. X. Gao and G. D. Zhou, *Corros. Sci.*, 2004, **46**(12), 3031–3040.
54 M. M. Kadhim, I. H. R. Tomi and A. A. Khadom, *J. Adhes. Sci. Technol.*, 2022, **37**(13), 1–18, DOI: **10.1080/01694243.2022.2086398**.
55 A. G. Bedir, M. Abd El-raouf, S. Abdel-Mawgoud, N. A. Negm and N. M. El Basiony, *ACS Omega*, 2021, **6**, 4300–4312.
56 A. A. Khadom, M. M. Kadhim, R. A. N. Anaee and A. W. Salman, *J. Mol. Liq.*, 2021, **343**(5), 116978.
57 M. A. A. Ibrahim, N. A. M. Moussa, A. H. M. Mahmoud, S. R. M. Sayed, P. A. Sidhom, M. K. Abd El-Rahman, T. Shoeib and L. A. Mohamed, *RSC Adv.*, 2023, **13**, 29023.
58 A. A. Khadom, S. A. Jassim, M. M. Kadhim and N. B. Ali, *J. Mol. Liq.*, 2022, **347**, 117984, DOI: **10.1016/j.molliq.2021.117984**.
59 M. Parveen, M. Mobin and S. Zehra, *RSC Adv.*, 2016, **6**, 61235–61248, DOI: **10.1039/C6RA10010D**.
60 G. A. Somorjai and M. A. Van Hove, *Introduction to Surface Chemistry and Catalysis*, John Wiley & Sons, 1997.
61 D. Frenkel and B. Smit, *Understanding Molecular Simulation: from Algorithms to Applications*, Academic Press, San Diego, CA, USA, 2002.
62 L. Guo, X. Ren, Y. Zhou, S. Xu and Y. Gong, Monte Carlo Simulations of Corrosion Inhibition of Copper by Two Schiff Bases, in *International Conference on Materials, Environmental and Biological Engineering (MEBE 2015)*, Atlantis Press, Amsterdam, The Netherlands, 2015.
63 M. M. Kamel, Q. Mohsen, Z. M. Anwar and M. A. Sherif, *J. Mater. Res. Technol.*, 2021, **11**, 875–886, DOI: **10.1016/j.jmrt.2021.01.055**.
64 Y. He, X. Wang, D. Young, M. Mohamed-Said, S. Ren and M. Singer, *J. Electrochem. Soc.*, 2023, **170**(11), 111502, DOI: **10.1149/1945-7111/ad09f6**.
65 M. M. Kamel, M. A. Ghanem, A. S. Fouda, S. M. Rashwan, O. Abdelkader, N. Y. Mostafa and K. M. H. Mohammed, *Egypt. J. Chem.*, 2024, DOI: **10.21608/EJCHEM.2024.277352.9465**.
66 G. N. Mu, T. P. Zhao, M. Liu and T. Gu, *Corrosion*, 1996, **52**(11), 853–856, DOI: **10.5006/1.3292077**.
67 O. U. Abakedi, V. N. Mkpenie and E. G. Ukpong, *Sci. Afr.*, 2020, **7**, e00256.
68 D. Mahalakshmi, V. Hemapriya, E. P. Subramaniam and S. Chitra, *J. Mol. Liq.*, 2019, **284**, 316–327.
69 B. A. Elsayed, M. A. Hegazy, H. M. H. Abd El-Bary and A. A. Abdel Salam, *Int. J. Adv. Eng. Nano Tech.*, 2016, **4**, 21–35.
70 T. Sethi, A. Chaturvedi, R. K. Upadhyay and S. P. Mathur, *J. Chil. Chem. Soc.*, 2007, **52**, 1206–1213.